Tellus SERIES A DYNAMIC METEOROLOGY AND OCEANOGRAPHY
PUBLISHED BY THE INTERNATIONAL METEOROLOGICAL INSTITUTE IN STOCKHOLM

Tellus (2008), 60A, 839–847
Printed in Singapore. All rights reserved

TELLUS

Equivalent finite volume and Eulerian spectral transform horizontal resolutions established from aqua-planet simulations

By DAVID L. WILLIAMSON*, *National Center for Atmospheric Research, Box 3000, Boulder, CO, USA*

(Manuscript received 19 September 2007; in final form 29 April 2008)

ABSTRACT

The equivalent resolutions for two different global dynamic cores are established when they are coupled to the sub-grid scale parametrization suite of the Community Atmosphere Model (CAM3). One core adopts the common Eulerian spectral transform formalism, the other adopts a finite volume approach. The equivalent resolutions are established over a range of resolutions employed today for climate models. The comparison is done in the context of the Aqua Planet Experiment (APE). Thus, it is based on the characteristics of free, unforced motions, due in large part to the dynamic component driven by the parametrized processes and explicit dissipation. The forced component arising from surface orography and land–ocean–sea–ice contrasts is not considered. The resolution equivalences are demonstrated for a number of model fields. These include selected time averaged, global and zonal averaged fields, the meridional structure of eddy kinetic energy and eddy temperature variance, the mean meridional eddy transports, the characteristics of tropical wave propagation and probability density functions of precipitation. These fields indicate that the 2° finite volume model is equivalent to T42 spectral transform model, 1° is equivalent to T85 and 0.5° is equivalent to T170. This proportional relationship does not hold at lower resolutions.

1. Introduction

For economic reasons, climate models are generally applied at low to moderate resolutions. Because of this, resolution can be a determining factor in model climate statistics, especially for properties other than the time-mean. Resolution itself might explain some of the common shortcomings in current climate models. However, to establish such a connection, equivalent resolutions of different numerical approaches must first be determined. A second reason to establish equivalent resolutions of numerical schemes is to allow a comparison of the cost of different numerical methods, which have the same accuracy and simulation characteristics.

Atmospheric models approximate the evolution of a modelled atmosphere, but are generally unable to resolve all processes involved. Models are conceptually divided into two components: a resolved dynamic fluid flow component which represents the atmospheric flow and an unresolved, sub-grid scale component, which is parametrized as functions of the large-scale, resolved flow. The parametrized component consists of radiative, planetary boundary layer, convective and stratiform cloud processes. The latter three include phase change of water and precipitation processes. These parametrized components provide a forcing to the resolved fluid flow and coupled with the dynamic component lead to a statistical equilibrium in long integrations—the model climate.

The discrete approximations to the resolved, fluid flow component of the model are generally referred to as the dynamic core and the sub-grid-scale component as the parametrization suite or more simply as the parametrizations. In non-linear fluid flow such as the atmosphere, enstrophy and energy cascade through the resolved scales and can accumulate at the truncation limit. In the continuous problem, these would normally continue to cascade to smaller and smaller scales until dissipated by friction. However, such dissipative processes occur in nature at scales well below those that can be included in models, and in the discrete system, energy can build up at the truncation limit. Terms to control this build-up or accumulation might naturally be thought of as another component of the parametrization suite since they deal with unresolved processes. However, some numerical methods help to control this accumulation through their inherent damping of small scales. This numerical artefact is difficult to separate from any explicitly designed damping mechanism. Thus, processes designed to prevent and control such build-up are generally considered to be part of the dynamic core. These can involve terms explicitly added to the equations

*Correspondence.
e-mail: wmson@ucar.edu
DOI: 10.1111/j.1600-0870.2008.00340.x

such as ∇^2 or ∇^4 diffusion of momentum and temperature, or damping that is implicitly designed into a numerical scheme, such as through monotonicity constraints.

It is difficult to determine equivalent resolutions of dynamic cores from first principles. For example, the shapes, as a function of wavenumber, of the linear response functions of discrete numerical operators can be very different for different numerical schemes, especially at the smaller resolved scales near the truncation limit. Durran (1999) provides examples of amplitude and phase response functions for many numerical methods. Minimum grid sizes are not necessarily relevant measures of accuracy, especially for non-linear applications. The response functions generally differ the most at the smallest scales, but the parametrizations interact with these small scales, as well as with the larger scales. In addition, the small scales interact with and affect the larger scales through the dynamical processes in a non-linear model.

Most analytic test cases commonly used to evaluate schemes tend to be rather simple deterministic tests. Even those which do not have analytic solutions and rely on very high resolution reference solutions tend to be relatively short, deterministic tests. Many tests are based on the shallow-water equations, e.g. Williamson et al. (1992). A few deterministic tests have been proposed recently as standards to evaluate baroclinic dynamic cores. These include Polvani et al. (2004), Jablonowski and Williamson (2006a) and Jablonowski and Williamson (2006b). There are, however, few tests to determine the relative quality of dynamic cores when coupled to parametrization suites after they have reached their climate statistical equilibrium regime, long after deterministic aspects of the evolving flow are lost.

The skill of weather forecasts made by a model might be considered a measure of overall accuracy, but one scheme may appear to be more skillful because errors in the parametrizations and in the dynamic core compensate or cancel each other. For the same reason, the skill in simulating current climate statistics is not a useful measure to evaluate the numerical component alone.

Establishing the equivalence of dynamic cores is further compounded by the observation that, at least in some models, resolution affects both the dynamic core and the parametrizations (Williamson, 1999). For example, the parametrizations in the community atmosphere model (CAM3) are in fact sensitive to resolution. In our experience, however, it is the resolution of the atmospheric flow that is crucial for the parametrizations, not the resolution of the underlying grid, even though the parametrizations are calculated on that grid. We have established this with the Eulerian spectral transform version of the CAM, where the atmospheric resolution is easily separated from the underlying Gaussian grid via the spectral truncation. For example, when a T42 truncation model is applied on a 256 × 128 point Gaussian grid instead of on the conventional 128 × 64 quadratically unaliased Gaussian grid, the properties we describe in the following match the properties from the T42 model on the 128 × 64 grid and not those from a T85 truncated model on its conventional 256 × 128 point quadratically unaliased grid. It is not as straightforward to perform a similar scale separation with a grid point model. Presumably, grid filters might be applied to the atmosphere flow before calculating the parametrizations, but the response functions of such filters are usually not as sharp as spectral truncation making the definition of the resulting resolution murky. Because the parametrization suite is dependent on the dynamic resolution, the parametrization resolution dependence should not be a problem in establishing the dynamic core resolution equivalence. The parametrizations should behave similarly at the dynamic resolutions found to be equivalent. In fact, the parametrizations might actually amplify the dynamic signal, making it easier to identify.

A component of the observed parametrization 'sensitivity to resolution' can be attributed to a sensitivity to the time step over which the parametrizations are calculated. When resolution is increased, many dynamic cores require smaller time steps for computational stability. The parametrizations are often applied at these shorter time steps. The combination dynamic core and parametrization suite appear to be sensitive to the time step (Williamson and Olson, 2003). However, they show that the sensitivity is due to the parametrizations and not the dynamic core. When the dynamic core is run with shorter time steps but the parametrizations retain the longer time step, the sensitivity is not seen. This is also the experience in numerical weather prediction (NWP). When semi-Lagrangian methods were developed and NWP models had minimal parametrizations, the forecasts were shown to be insensitive in any significant way to time step (Staniforth and Côté, 1991). Therefore, all the experiments discussed in this paper apply the same time step for the parametrization suite.

It is unlikely that the solutions produced by two numerical schemes will be exactly equivalent in all aspects. Here we look for resolution pairs that produce equivalences in general characteristics of the statistical model climates. To be able to identify any such equivalence, there must be a systematic signal as a function of resolution. In a companion paper (Williamson, 2008), we study the convergence characteristics of the Eulerian spectral transform model used in this paper and identify such consistent signals. That paper also identifies minimum resolutions needed to capture certain large-scale aspects of the simulations. In the conclusions, here we mention implications of other aspects of the numerical schemes that modelling groups take into consideration when defining their model. These are the overall cost and inherent physical properties such as conservation and shape preservation.

2. Model description

In the following, we establish the equivalent resolutions for two very different dynamic cores: one based on the traditional Eulerian spectral transform method (Machenhauer, 1979) and

the other based on finite volume approximations (Lin and Rood, 1997). The equivalence is established over a range of resolutions employed today for climate models. The Eulerian spectral transform core is the default core in the CAM3 and the finite volume core is an option included with the code for future development. The CAM3 was developed as the atmospheric component of the community climate system model (CCSM3), where it is coupled to active ocean, land and sea ice models (Collins et al., 2006a). The CAM3 can also be run in a stand-alone mode with specified sea surface temperatures (SST) and sea ice extent, while coupled to an active land model. An overview of the CAM3 is provided by Collins et al. (2006b) and a complete technical description of CAM3, including the standard and two optional dynamic cores, by Collins et al. (2004). For the spectral transform core we consider T42, T85, T170 and T340 truncations. For the finite volume, we consider latitude $\times$ longitude grids of $2^\circ \times 2.5^\circ$, $1^\circ \times 1.25^\circ$ and $0.5^\circ \times 0.625^\circ$. We refer to these as 2°, 1° and 0.5° grids, respectively. For all experiments, we use the standard 26-level vertical grid of the default model. In all cases, the parametrization time step is 5 min, the shortest required by the dynamic cores with the resolutions considered here. Parametrization packages are often tuned in climate models for different horizontal resolutions (Hack et al., 2006). Such changes affect the simulated climates. To avoid introducing such an effect into our experiments, we use the same parameter settings in the parametrization suite for all experiments, namely those of the T85 spectral transform model given in Hack et al. (2006). As mentioned above, dynamic cores generally include some mechanism to control the build-up of energy in the small-scales near the truncation limit. The spectral transform core includes a ∇^4 diffusion of vorticity, divergence and temperature. In the finite volume core, the smallest scales are controlled to some extent by the monotonicity constraints of the numerical scheme. However, the divergence is not well controlled by that mechanism, and a ∇^2 diffusion is applied to the divergence. The values of the coefficients used here, which are different for each resolution, and additional details of the terms are given in Jablonowski and Williamson (2006a).

3. Idealized test case

Before discussing our experiments, we review a related comparison involving an idealized test case for dynamic cores. The results of Jablonowski and Williamson (2006a) for an idealized growing baroclinic wave test case show that T85 and 1° are the lowest resolutions for the spectral transform core and the finite volume core, respectively, that capture the reference solutions to within their uncertainty. The T42 spectral transform and the 2° finite volume cores do not capture the reference solutions and the l_2 difference norms calculated against a reference solution are similar to each other. This is the first indication that T42 versus 2° and T85 versus 1° provide two equivalent resolution pairs for those cores. Jablonowski and Williamson (2006b) show maps of the growing perturbations at a fixed elapsed time. The above equivalences can be seen visually there. The maps for resolutions higher than T85 and 1° all look similar to those of T85 and 1°. Therefore, we cannot draw conclusions from that test about equivalences of higher resolution models. The maps for T42 and 2° look very similar. However, the maps for resolutions lower than T42 and 2° look very different. The T21 spectral transform core captures about half the amplitude of the growing wave of the reference solutions, whereas the 4° finite volume core has very minimal amplitude. Although not explicitly discussed in Jablonowski and Williamson (2006a) and Jablonowski and Williamson (2006b), it is not the case that the 4° finite volume core simply has a slower growth rate but ultimately captures the larger amplitude at later times. If that were the case, the T21 spectral transform and 4° finite volume cores might produce equivalent eddy statistics in a forced model at climate equilibrium. But, in fact, the wave in the 4° finite volume core simply does not grow significantly in amplitude. Therefore, we conclude that T21 versus 4° is not an equivalent resolution pair.

4. Experimental design

The results described above are for an idealized baroclinic instability test case. The question remains as to whether those results are relevant for more atmosphere-like situations in which a climate equilibrium is established when the cores are forced by a sub-grid scale parametrization suite. In the remainder of this paper, we consider statistical aspects of the model climate produced by the dynamic cores coupled to the CAM3 parametrization suite. We base our comparison on the characteristics of free, unforced motions, which are due, in large part, to the dynamic component driven by the parametrized processes and explicit dissipation. The comparison is done in the context of the aqua planet experiment (APE; website: http://www.met.reading.ac.uk/∼mike/APE/) based on standard experiments set by Neale and Hoskins (2000). The aqua-planet approach includes the full complexity of the atmospheric model including the parametrization suite, but simplifies the lower boundary exchange by defining a less complex surface. The aqua-planet earth is covered with water and has no mountains, land or sea ice. The sea surface temperatures (SST) are specified, usually with rather simple geometries such as zonal symmetry as in our case. A diurnal cycle in radiation is included with the sun remaining over the equator. Since there is no land-sea contrast, no mountains and no longitudinal variation in the SST, there is no forced component of the solutions, and as mentioned above, the climate consists primarily of free motions. The 'correct' solutions of aqua-planet tests are not known. Nevertheless they have proven useful for a variety of studies involving parametrizations and dynamic cores.

Our following study is based on the 'CONTROL' case defined by Neale and Hoskins (2000) in which the zonal SST in $^\circ$C is given by $27[1 - \sin^2(3\varphi/2)]$ for latitude φ between $+\pi/3$

and $-\pi/3$ and 0 elsewhere. This field is well represented by the lowest spectral resolution we consider. The maximum difference between the field truncated to T42 and the analytic field is of the order of 0.0005 K, giving about 5 digits of agreement. The simulations start from data interpolated from a previous aqua-planet simulation and are run for 14 months. The analyses are over the last 12 months. The first two months are more than adequate for the model to transition to its own climate regime. We have run a few of the lower resolution cases longer and established that 12 month samples are adequate for the statistics considered here, although we do not perform statistical significance testing in this paper. The highest resolution simulations were to expensive to run longer to allow that.

In the following sections, we compare a variety of statistical quantities from the aqua-planet climate equilibrium. Because the idealized baroclinic instability test case indicated that T21 versus 4° is not an equivalent resolution pair, we do not consider resolutions below T42 for the spectral transform core or below 2° for the finite volume core. The comparison will demonstrate resolution equivalences for a number of key model fields. These are global averages, zonal averages, the meridional structure of eddy kinetic energy and eddy temperature variance, mean meridional eddy transports, characteristics of tropical wave propagation and probability density functions of precipitation in the equatorial region and in mid-latitudes. We conclude that in general the 2° finite volume model is equivalent to T42 spectral transform model, 1° is equivalent to T85 and 0.5° is equivalent to T170. We will refer to these as proposed equivalent resolution pairings. As we will see, the pairings are not exact since we consider resolution changes of a factor of 2 only and nothing in between. The chosen resolutions are those that have been commonly used for CAM3 applications.

5. Global averages

Figure 1a shows the time average, global average precipitable water, the solid bars from the spectral transform core and the hatched from the finite volume. The global average decreases with increasing resolution. The proposed resolution parings—(2°, T42), (1°, T85) and (0.5°, T170)—stand out even with the modest variation with resolution that occurs in this field. (Note that the ordinate starts at half of the maximum value to exaggerate the variation). In fact, given the resolution trend, each finite volume value would probably match values from a slightly lower spectral transform resolution than the ones sampled here. Figure 1b shows the time average, global average total precipitation and its two components: convective and stratiform or stable. The total precipitation increases with increasing resolution. The components have opposite resolution signals with convective decreasing and stable increasing with increasing resolution. In each case, the proposed parings hold, but again the finite volume values would probably match values produced by a slightly lower spectral transform resolution if one were looking for exact equivalence.

6. Zonal averages

Figure 2 shows graphs of the time average, zonal average surface pressure, zonal surface stress and cloud fraction. Since the forcing and resulting zonal averages are symmetric about the equator, the two hemispheres are averaged to reduce the sampling variability slightly. Consider first the surface pressure, which represents the mass of the atmosphere. By model design, the global average of the surface pressure is essentially the same for all these simulations. The only variation is due to the difference in precipitable water seen in Fig. 1a and that is within the thickness of the lines plotted here with this scale. Figure 2a shows that there is a shift in the mass from polar to equatorial regions with increasing resolution, and the latitude of the minimum surface pressure moves slightly poleward. The proposed resolution pairings are also seen here—(2°, T42), (1°, T85) and (0.5°, T170)—with finite volume again representing a slightly lower resolution than the proposed pairings. The mass shift with resolution has implications for the poleward transport of angular

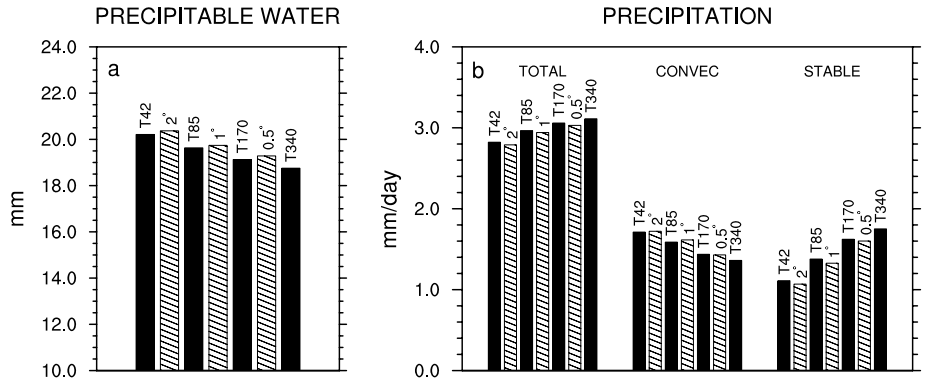

Fig. 1. Time average, global average of (a) precipitable water, and (b) precipitation for T42, T85, T170 and T340 spectral and 2°, 1° and 0.5° finite volume models.

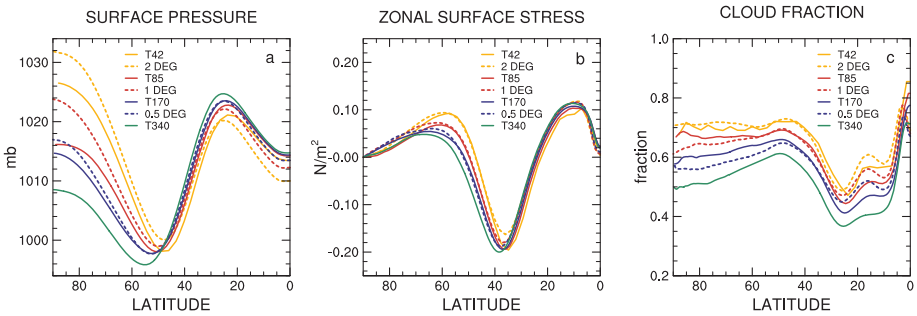

Fig. 2. Time average, zonal average of (a) surface pressure, (b) zonal surface stress and (c) cloud fraction for T42, T85, T170 and T340 spectral and 2°, 1° and 0.5° finite volume models.

momentum and its effect on the mid-latitude westerly winds and easterly trade winds. These are discussed in a companion paper (Williamson, 2008).

Figure 2b shows the zonal surface stress. Again, there is a monotonic signal with increasing resolution. For this field, the proposed pairings are much closer. Figure 2c shows the total cloud fraction. In mid- to high-latitudes the resolution parings hold, but now with the finite volume representing a slightly higher resolution poleward of 60° but not as high as the next spectral transform resolution considered. The two models differ slightly in structure in the equatorial region. Although it is difficult to discern in the figure, the finite volume core forms a double ITCZ with minima on the equator and maxima just off the equator whereas the spectral transform core forms a single ITCZ with maxima on the equator. The cause of this structural difference has not yet been established, and one wonders how high a resolution is needed for the solutions to converge there. We note in passing that all the finite volume grids have a grid point on the equator but none of the spectral transform grids do. In addition, in the finite volume approximations, the horizontal wind components and temperature and water vapour variables are staggered in the horizontal grid; in the Eulerian spectral transform approximations they are not.

7. Meridional eddy statistics

In this section, we consider zonal averaged eddy statistics which reflect the baroclinic wave activity in the climate equilibrium. Denote the time mean of a variable ψ by an overbar, $\overline{\psi}$, and deviations from the time mean by a prime, $\psi' = \psi - \overline{\psi}$. In the following, we compare the zonal averaged eddy temperature variance, $\overline{(T')^2}$, eddy kinetic energy, $\frac{1}{2}[\overline{(u')^2} + \overline{(v')^2}]$, meridional eddy momentum flux, $\overline{(v'u')}$, and meridional eddy heat flux, $\overline{(v'T')}$. Figure 3 shows zonal averages of these quantities as a function of latitude at selected pressure levels. Again, the two hemispheres are averaged to reduce the noise, symmetrically for symmetric fields and antisymmetrically for antisymetric ones.

Figure 3a shows the eddy temperature variance at 200mb. There is a strong monotonic resolution signal with the maximum at 40°, increasing in both models with increasing resolution. The T42 and 2° agree quite well, as do the T85 and 1°. The T170 and T340 values imply the field has converged, but the 0.5° value is a little less than the T170. Figure 3b shows the eddy kinetic energy at 300 mb. Again, there is a monotonic increase with increasing resolution, but the peak value in the finite volume around 40° is a little smaller than that from the spectral for each resolution pair. Figure 3c shows the eddy kinetic energy at 200 mb. The behaviour is less monotonic at this level. With the spectral, the maximum values at 35° increase from T42 to T85, then decrease monotonically to T170 and T340 (The T42 yellow line is difficult to discern, being under the dashed red 1° line in the region of the maxima). With the finite volume, the maximum values increase from 2° to 1° to 0.5°. In all cases, the finite volume is weaker than the corresponding spectral, most notably with the (2°, T42) pair.

Figure 3d shows the meridional momentum flux at 300 mb. Here again, there is a monotonic signal with increasing resolution and the proposed resolution pairings are very clear. Figure 3e shows the meridional momentum flux at 200 mb. The correspondences are clear, but the finite volume maxima occur slightly more poleward and with slightly lower amplitude in the lower resolutions. Finally, Fig. 3f shows the meridional heat flux at 800 mb. The higher resolutions have very similar values, but for all resolution pairs, the finite volume is lower than the corresponding spectral, most notably at T42 and 2°, but being just discernible at the higher resolution pairings.

In all fields examined, the proposed resolution pairings hold in general, with perhaps the finite volume being given the benefit of the doubt, that is, it may be equivalent to a slightly lower resolution spectral transform core, but we have not investigated resolutions in between those of the doubling sequences presented here.

8. Equatorial wave propagation

The equatorial wave propagation characteristics of the simulations are compared via wavenumber-frequency spectrum analysis following the methodology of Wheeler and Kiladis (1999). Figure 4 plots the symmetric component of the unnormalized power spectra of the precipitation averaged from 10°S to 10°N.

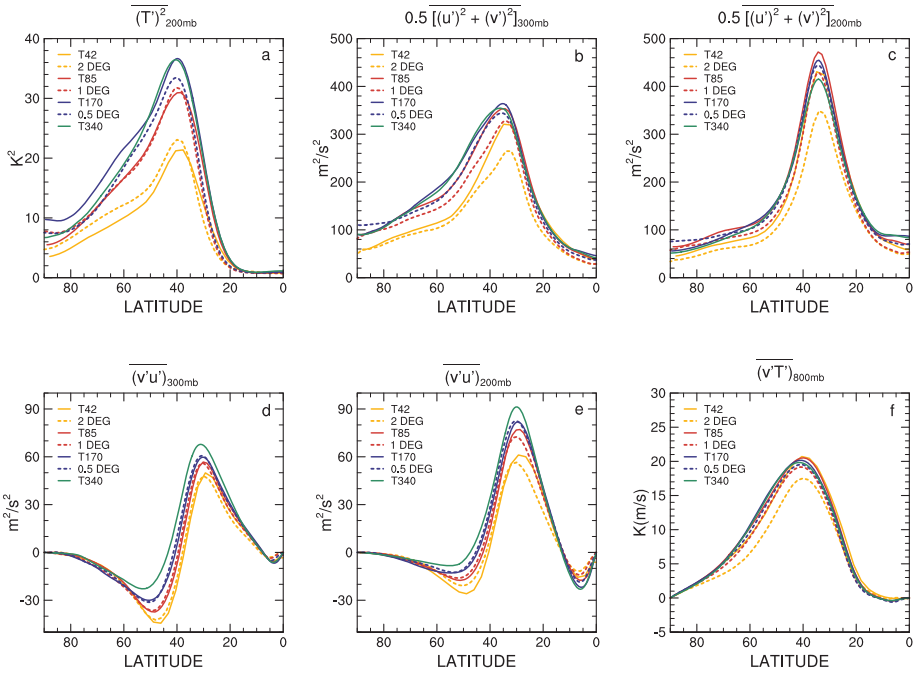

Fig. 3. Zonal average eddy temperature variance, $\overline{(T')^2}$, at 200 mb (a); eddy kinetic energy, $\frac{1}{2}[\overline{(u')^2 + (v')^2}]$, at 300 mb (b) and 200 mb (c); meridional eddy momentum flux, $\overline{(v'u')}$ at 300 mb (d) and 200 mb (e) and meridional eddy heat flux, $\overline{(v'T')}$, at 800mb (f) for T42, T85, T170 and T340 spectral and 2°, 1° and 0.5° finite volume models.

Interesting signals can be seen without removing a background spectrum, allowing a comparison of the overall power of the waves. The Wheeler and Kiladis type normalization isolates spectral peaks that are often associated with specific normal modes or waves, but since the normalization is done individually for each model, the overall resolution signal associated with the power is lost to the 'background' spectrum. Figure 4 includes the conventional dispersion curves for odd meridional mode-numbered equatorial waves for equivalent depths of 12, 25 and 50 m. The curves in the upper half of the plots show westward and eastward propagating inertio-gravity waves. The diagonal lines to the right-hand side are the eastward propagating Kelvin modes and the lower curves to the left-hand side are the westward propagating equatorial Rossby waves. In each set, the period decreases with increasing equivalent depth.

The left-hand column of Fig. 4, top to bottom, shows the power from the spectral simulations for T42, T85, T170 and T340. The power increases with increasing resolution, most notably from T42 to T85, but from T85 to T170 as well. T340 looks quite similar to T170, perhaps indicating convergence, at least to within the noise present in these relatively short samples. T42 shows a belt of increased power above the 50 m equivalent-depth Kelvin mode line. This also shows up in a normalized plot (not shown). There is also an isolated eastward propagating wavenumber 6 peak, with period between 6 and 10 d. There is a significant increase in power going from T42 to T85 at all periods and wavenumbers. The belt of increased power associated with Kelvin modes seen in T42 is not notable in T85, nor is the isolated wavenumber 6 feature. Comparing T170 with T85 shows an increase in power along the 25 m equivalent-depth Kelvin mode line. The T85 and higher resolutions also show a block of power, covering wavenumber 0 and eastward wavenumbers 1 and 2 with period between 15 and 30 d, which is missing from the T42. Such power is often associated with the MJO, but it usually includes higher wavenumbers. Also the inclusion of wavenumber 0 is unusual. The normalized signal (not shown) strengthens only slightly from T85 to T170. We also note that all resolutions show a very low-frequency eastward propagating wavenumber 5. The one-year samples are too short to allow comparison of the amplitude of this feature.

The right-hand column of Fig. 4, top to bottom, shows the power from the 2°, 1° and 0.5° finite volume simulations. The proposed resolution equivalences seem rather close, but the finite volume has slightly lower power than the equivalent spectral, implying the finite volume is equivalent to a slightly lower spectral resolution but certainly not a factor of two. The 2° shows the increased power above the 50 m equivalent-depth Kelvin mode line seen in the T42, as well as the isolated eastward propagating wavenumber 6 peak with period between 6 and 10 d. The power in each is slightly less than the T42. The wavenumber 6 peak remains visible in the 1° but is gone in the 0.5°. The 0.5° does not capture the increase in power along the 25 m equivalent-depth Kelvin mode line that is seen in the T170. Again, this implies the finite volume is equivalent to a slightly lower spectral

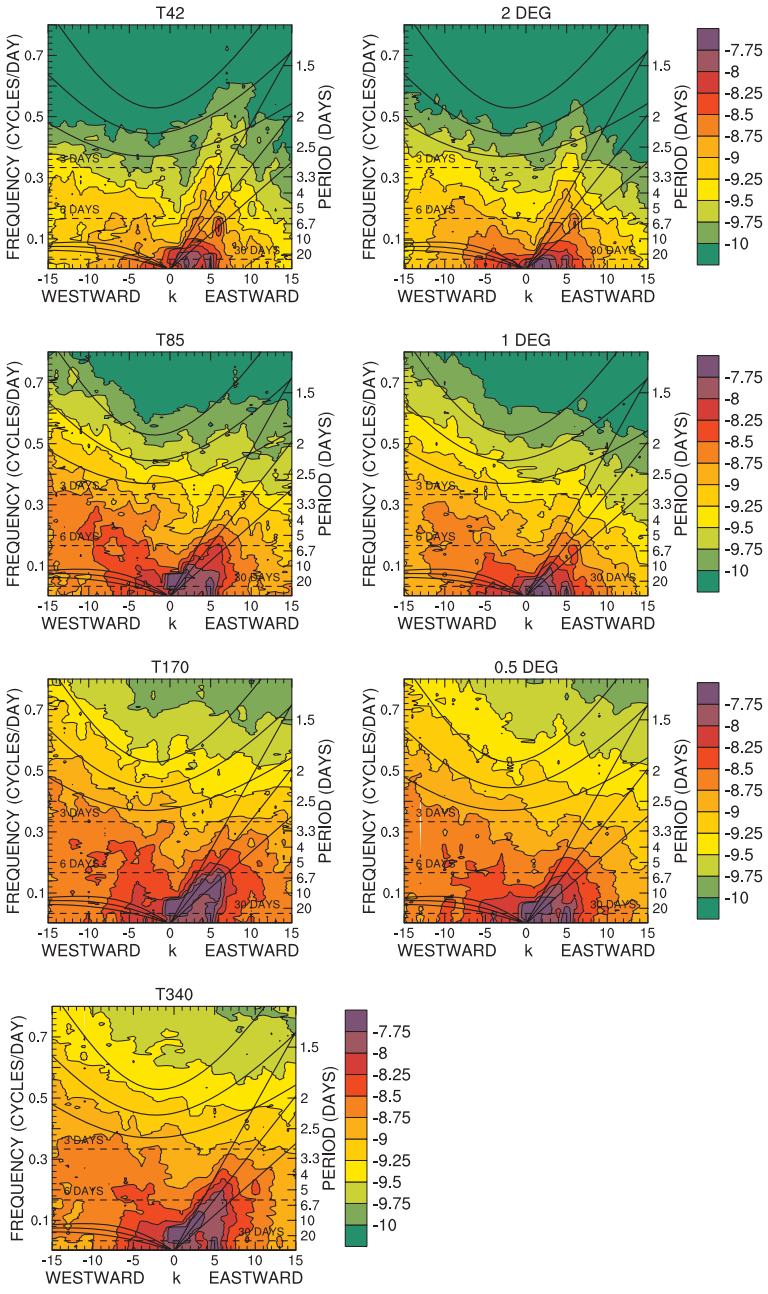

Fig. 4. Wavenumber-frequency diagram showing the symmetric component of the unnormalized power spectra of the precipitation averaged from 10°S to 10°N for T42, T85, T170 and T340 spectral model (left-hand column) and 2°, 1° and 0.5° finite volume model (right-hand column).

resolution than the proposed pairings: (T42, 2°), (T85, 1°) and (T170, 0.5°).

9. Probability density function of precipitation

The final resolution comparison we show is the probability density function of 6-h averaged precipitation in the equatorial region calculated from all grid points between 10°S to 10°N. To emphasize the smaller rainfall rates, the left-hand side panel of Fig. 5 shows the fraction of the time the precipitation is in each 1 mm d^{-1} bin ranging from 0 to 120 mm d^{-1}. To emphasize the larger values, the right-hand side panel shows the fraction of the time the precipitation is in each 10 mm d^{-1} bin ranging from 0 to 1200 mm d^{-1}. In each case, the left-most bin is the fraction of the time the precipitation is exactly 0, and the right-most, the fraction of time the precipitation exceeds 120 or 1200 mm d^{-1}. Once again a clear resolution signal is seen, and the resolution association is clear. For this field, the finite volume appears equivalent to a slightly higher spectral resolution than our proposed pairings, but only by a small factor. There is a clear separation between the resolution pairings. We obtain similar results for mid-latitudes, between 25° and 45°, except

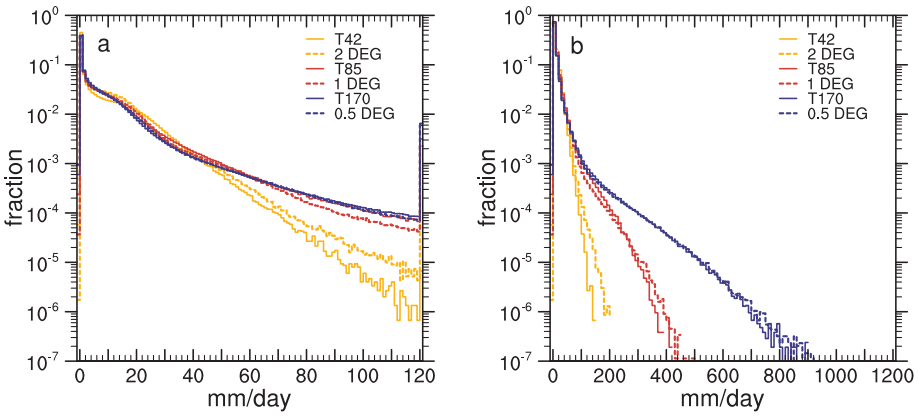

Fig. 5. Fraction of the time the precipitation is in 1 mm d^{-1} bins ranging from 0 to 120 mm d^{-1} (left-hand side) and in 10 mm d^{-1} bins ranging from 0 to 1200 mm d^{-1} (right-hand side), calculated from six-hour averages for all grid points between $\pm 10^\circ$ latitude for T42, T85, T170 and T340 spectral and 2°, 1° and 0.5° finite volume model.

there is less variation with resolution in the probability of large values (not shown).

10. Conclusions

We have established the equivalent resolutions for two very different dynamic cores: one based on a traditional Eulerian spectral transform method (Machenhauer, 1979) and the other on finite volume approximations (Lin and Rood, 1997). The dynamic cores are documented in Collins et al. (2004). Equivalent resolution pairs are established over a range of resolutions employed today for climate models. The comparison is done in the context of an APE. The aqua-planet approach includes the full complexity of the atmospheric model including the parametrization suite, but simplifies the lower boundary exchange by specifying the temperature of a water covered surface. The parametrization suite coupled to both cores is that of the CAM3 (Collins et al., 2006b). For the experiments here, the CONTROL case of Neale and Hoskins (2000) is used in which the sea surface temperatures are zonally symmetric with a meridional distribution that is well resolved by the lowest resolutions considered here, namely T42 for the Eulerian spectral transform and 2° for the finite volume. Since the aqua-planet has no land–sea contrast, no mountains and no longitudinal variation in the SST, there is no forced component of the solutions. The climate produced by such a scenario consists primarily of free motions. Since the parametrization suite is sensitive to time step, the same time step is used for all experiments. In addition, the same parameter settings are invoked in the parametrization suite for both cores at all resolutions. That is, the parameters are not tuned to produce a best climate, especially since a theoretical climate of the aqua-planet is not known. The Eulerian spectral transform based model is applied at T42, T85, T170 and T340 truncations on approximately 2.8°, 1.4°, 0.7° and 0.35° transform grids, respectively. The finite volume based core is applied on latitude × longitude grids of 2° × 2.5°, 1° × 1.25° and 0.5° × 0.625°.

We demonstrate the resolution equivalences for a number of key model statistics. These are selected time average, global and zonal averages, the meridional structure of eddy kinetic energy and eddy temperature variance, mean meridional eddy transports, characteristics of tropical wave propagation and probability density functions of precipitation in the equatorial region and in mid-latitudes. For all statistics considered, we find that for the resolutions considered, the 2° finite volume model is closest to the T42 spectral transform model, 1° is closest to T85 and 0.5° is closest to T170. We note that these pairings are not exact since we consider resolution changes of a factor of 2 only and none in between. But the statistics of these pairs are quite close and certainly not midway between resolutions. Thus, we conclude that (2°, T42), (1°, T85) and (0.5°, T170) are equivalent resolution pairs for these dynamic cores. We note that this proportional relationship does not hold at lower resolution. Results from the idealized baroclinic instability test case of Jablonowski and Williamson (2006a,b) indicate that the 4° finite volume core is not equivalent to the T21 spectral transform core.

The equivalent resolution pairs have been established only for these two particular dynamic cores as implemented in the CAM. One should not draw general conclusions from this analysis for other dynamic cores. For instance, a semi-Lagrangian spectral transform dynamic core is also available in the CAM. We have not examined it in this equivalence context. One should not automatically assume that it is equivalent to the Eulerian spectral transform core at the same resolution since at lower resolutions, general experience is that the semi-Lagrangian approximations are more diffusive than the Eulerian. Similarly, staggered and unstaggered grids with the same nominal grid resolutions might not result in equivalent climates in the sense considered here.

The resolution equivalence has only been established in terms of general characteristics of the model simulations. There are other characteristics of the dynamic cores that might set the schemes apart. Efficiency is one while maintaining some basic physical properties in the approximations is another. In the

CAM implementation, when the parametrizations are applied at the same time step, the Eulerian spectral transform model requires less computer time than the finite volume for an equivalent resolution pair. The parametrization suite dominates the models costs in terms of computer time, and for any pair, the finite volume has more grid points on which the parametrizations are calculated. To first order, the ratio of the costs of the models is nearly proportional to the ratio of the number of grid points. On the other hand, the finite volume approximations incorporate desirable physical properties that the Eulerian spectral does not. These include local flux based conservation of advected tracers and monotonic or shape preserving conditions. In spite of the higher cost, the NCAR CCSM is adopting the finite volume dynamic core for its next release to have conservative and shape preserving transport for chemical species. It is felt that those properties are worth the extra cost.

Finally, we note that these resolution equivalences have been established with the CAM3 parametrization suite. It is possible that they depend on the forcing from the parametrization suite and that a different set of parametrizations might yield slightly different results. In addition, the simulations do not include a strongly forced component from surface orography or land-sea contrasts. The forced component in a complete general circulation model might have different properties, especially as the scales of such forcing generally decrease with increasing resolution. Nevertheless, one would expect the free component properties of the complete system to be similar to those studied here.

11. Acknowledgments

I would like to thank Jerry Olson for developing the required code and running the experiments. The anonymous reviewers provided useful comments. This research was partially supported by the Office of Science (BER), U.S. Department of Energy, Cooperative Agreement No. DE-FC02-97ER62402. The National Center for Atmospheric Research is sponsored by the National Science Foundation.

References

Collins, W. D., Rasch, P. J., Boville, B. A., Hack, J. J., McCaa, J. R. and co-authors. 2004. Description of the NCAR community atmosphere model (CAM3.0). NCAR Technical Note NCAR/TN-464+STR, xii+214 pp.

Collins, W. D., Bitz, C. M., Blackmon, M. L., Bonan, G. B., Bretherton, C. S. and co-authors. 2006a. The community climate system model version 3 (CCSM3). *J. Climate* **19**, 2122–2143.

Collins, W. D., Rasch, P. J., Boville, B. A., Hack, J. J., McCaa, J. R. and co-authors. 2006b. The formulation and atmospheric simulation of the community atmosphere model version 3 (CAM3). *J. Climate* **19**, 2144–2161.

Durran, D. R. 1999. *Numerical Methods for Wave Equations in Geophysical Fluid Dynamics*. Springer, New York , 465 pp.

Hack, J. J., Caron, J. M., Danabasoglu, G., Oleson, K. W., Bitz, C. M. and co-authors. 2006. CCSM CAM3 climate simulation sensitivity to changes in horizontal resolution. *J. Climate* **19**, 2267–2289.

Jablonowski, C. and Williamson, D. L. 2006a. A baroclinic wave test case for dynamical cores of general circulation models: model intercomparisons. NCAR Technical Note NCAR/TN-469+STR available online at http://www.library.ucar.edu/uhtbin/hyperion-image/DR000790.

Jablonowski, C. and Williamson, D. L. 2006b. A baroclinic instability test case for atmospheric model dynamical cores. *Quart. J. Roy. Meteor. Soc.* **132**, 2943–2976.

Lin, S. and Rood, R. B. 1997. An explicit flux-form semi-Lagrangian shallow-water model on the sphere. *Quart. J. Roy. Meteor. Soc.* **123**, 2477–2498.

Machenhauer, B. 1979. The spectral method. In: *Numerical Methods Used in Atmospheric Models* Volume 2, GARP Publications Series No. 17, (ed. A. Kasahara), WMO and ICSU, Geneva , 121–275.

Neale, R. B. and Hoskins, B. J. 2000. A standard test for AGCMs including their physical parameterizations, I: the proposal. *Atmos. Sci. Lett.* **1**, 101–107 available online at http://www.idealibrary.com/links/doi/10.1006/asle.2000.0019.

Polvani, L. M., Scott, R. K. and Thomas, S. J. 2004. Numerically converged solutions of the global primitive equations for testing the dynamical core of atmospheric GCMs. *Mon. Wea. Rev.* **132**, 2539–2552.

Staniforth, A. and Côté, J. 1991. Semi-Lagrangian integration schemes for atmospheric models – a review. *Mon. Wea. Rev.* **119**, 2206–2223.

Wheeler, M. C. and Kiladis, G. N. 1999. Convectively coupled equatorial waves: Analysis of clouds and temperature in the wavenumber-frequency domain. *J. Atmos. Sci.* **56**, 374–399.

Williamson, D. L. 1999. Convergence of atmospheric simulations with increasing horizontal resolution and fixed forcing scales. *Tellus* **51A**, 663–673.

Williamson, D. L. 2008. Convergence of aqua-planet simulations with increasing resolution in the community atmospheric model, Version 3. *Tellus* **60A**, doi:10.1111/j.1600-0870.2008.00339.x.

Williamson, D. L. and Olson, J. G. 2003. Dependence of aqua-planet simulations on time step. *Quart. J. Roy. Meteor. Soc.* **129**, 2049–2064.

Williamson, D. L., Drake, J. B., Hack, J. J., Jakob, R. and Swarztrauber, P. N. 1992. A standard test set for numerical approximations to the shallow water equations in spherical geometry. *J. Comput. Phys.* **102**, 211–224.